# Preclinical Development of [$^{211}$At]meta-astatobenzylguanidine ([$^{211}$At]MABG) as an Alpha Particle Radiopharmaceutical Therapy for Neuroblastoma

Vandana Batra[1,2], Minu Samanta[1], Mehran Makvandi[3], David Groff[1], Paul Martorano[3], Jimmy Elias[1], Pietro Ranieri[1], Matthew Tsang[1], Catherine Hou[3], Yimei Li[2,4], Bruce Pawel[5], Daniel Martinez[6], Ganesan Vaidyanathan[7], Sean Carlin[3], Daniel A. Pryma[2,3], and John M. Maris[1,2]

## ABSTRACT

**Purpose:** [$^{131}$I]meta-iodobenzylguanidine ([$^{131}$I]MIBG) is a targeted radiotherapeutic administered systemically to deliver beta particle radiation in neuroblastoma. However, relapses in the bone marrow are common. [$^{211}$At]meta-astatobenzylguanidine ([$^{211}$At]MABG) is an alpha particle emitter with higher biological effectiveness and short path length which effectively sterilizes microscopic residual disease. Here we investigated the safety and antitumor activity [$^{211}$At]MABG in preclinical models of neuroblastoma.

**Experimental Design:** We defined the maximum tolerated dose (MTD), biodistribution, and toxicity of [$^{211}$At]MABG in immunodeficient mice in comparison with [$^{131}$I]MIBG. We compared the antitumor efficacy of [$^{211}$At]MABG with [$^{131}$I]MIBG in three murine xenograft models. Finally, we explored the efficacy of [$^{211}$At]MABG after tail vein xenografting designed to model disseminated neuroblastoma.

**Results:** The MTD of [$^{211}$At]MABG was 66.7 MBq/kg (1.8 mCi/kg) in CB17SC *scid*$^{-/-}$ mice and 51.8 MBq/kg (1.4 mCi/kg) in NOD.Cg-*Prkdc*$^{scid}$ *Il2rg*$^{tm1Wjl}$/SzJ (NSG) mice. Biodistribution of [$^{211}$At]MABG was similar to [$^{131}$I]MIBG. Long-term toxicity studies on mice administered with doses up to 41.5 MBq/kg (1.12 mCi/kg) showed the radiotherapeutic to be well tolerated. Both 66.7 MBq/kg (1.8 mCi/kg) single dose and fractionated dosing 16.6 MBq/kg/fraction (0.45 mCi/kg) × 4 over 11 days induced marked tumor regression in two of the three models studied. Survival was significantly prolonged for mice treated with 12.9 MBq/kg/fraction (0.35 mCi/kg) × 4 doses over 11 days [$^{211}$At]MABG in the disseminated disease (IMR-05$^{NET/GFP/LUC}$) model ($P = 0.003$) suggesting eradication of microscopic disease.

**Conclusions:** [$^{211}$At]MABG has significant survival advantage in disseminated models of neuroblastoma. An alpha particle emitting radiopharmaceutical may be effective against microscopic disseminated disease, warranting clinical development.

## Introduction

Approximately half of the patients with high-risk neuroblastoma are not cured with existing multimodality treatments, and more effective therapies are urgently needed (1, 2). Neuroblastoma is a radiosensitive embryonal malignancy derived from neural crest progenitor cells of the developing sympathetic nervous system. About 85% of neuroblastomas abundantly express the lineage-restricted norepinephrine transporter (NET; derived from the *SLC6A* gene) on the cell surface (3, 4). [$^{131}$I]meta-iodobenzylguanidine ([$^{131}$I]MIBG), a radioactive substrate for NET that is administered systemically to deliver β-particle radiation directly to neuroblastoma cells (5, 6) is currently in phase III testing for neuroblastoma (NCT03126916), and is FDA approved for the treatment of NET-overexpressing pheochromocytoma or paraganglioma. [$^{131}$I]MIBG has been shown to have single-agent response rates of 30% to 40% in patients with relapsed neuroblastoma (7–9), and the availability of sensitive and specific imaging with [$^{123}$I]MIBG allows for careful selection of patients for [$^{131}$I]MIBG therapy and monitoring of antitumor response.

Despite the overall impressive activity of [$^{131}$I]MIBG in this disease, responses are typically transient. This is thought to be due in large part to the fact that β-particles like those from $^{131}$I are suboptimal for killing isolated cells, or small cell clumps, due to their long path lengths. This is inferred from the fact that majority of treatment failures are in the bone marrow compartment (2, 10), where we hypothesize that the long path length of the β-particle emitted by $^{131}$I (millimeters) is ineffective in eliminating micrometastatic disease. In addition, β-particles have a long range in tissues and deposit their energy over several millimeters. The fraction of absorbed radiation dose in tumor decreases with the decreasing size of the tumor. The calculated ratio of fractional

[1]Division of Oncology and Center for Childhood Cancer Research, Children's Hospital of Philadelphia, Philadelphia, Pennsylvania. [2]Perelman School of Medicine at the University of Pennsylvania, Philadelphia, Pennsylvania. [3]Department of Radiology, University of Pennsylvania, Philadelphia, Pennsylvania. [4]Department of Biostatistics, Epidemiology, and Informatics, Perelman School of Medicine at the University of Pennsylvania, Philadelphia, Pennsylvania. [5]Department of Pathology and Laboratory Medicine, Children's Hospital Los Angeles and Keck School of Medicine, University of Southern California, Los Angeles, California. [6]Division of Anatomic Pathology, Children's Hospital of Philadelphia, Philadelphia, Pennsylvania. [7]Department of Radiology, Duke University Medical Center, Durham, North Carolina.

V. Batra and M. Samanta contributed equally to this article.

**Corresponding Author:** John M. Maris, Division of Oncology and Center for Childhood Cancer Research, Children's Hospital of Philadelphia, 3501 Civic Center Boulevard, Philadelphia, PA 19104. Phone: 215-590-5242; E-mail: maris@chop.edu

Clin Cancer Res 2022;28:4146–57

**doi:** 10.1158/1078-0432.CCR-22-0400

This open access article is distributed under the Creative Commons Attribution-NonCommercial-NoDerivatives 4.0 International (CC BY-NC-ND 4.0) license.

©2022 The Authors; Published by the American Association for Cancer Research

## Translational Relevance

Neuroblastoma is a radiosensitive malignancy that typically expresses the norepinephrine transporter (NET) at high levels. [$^{131}$I]MIBG is a NET ligand and effective targeted radiotherapeutic, but relapse, especially in the bone marrow compartment, is common. Here we show that [$^{211}$At]MABG, an alpha particle emitting radiopharmaceutical, shows comparable efficacy to [$^{131}$I]MIBG in preclinical models of neuroblastoma. Alpha particle emission leads to lethal ionization damage to DNA and targets isolated cancer cells and regresses small metastatic cancer cell clusters. Clinical experience with [$^{131}$I]MIBG highlights its efficacy in necrosis of soft-tissue masses. Thus. the two radionuclides have potentially complementary roles in neuroblastoma. These data support the clinical development of [$^{211}$At]MABG as a radiotherapeutic that would be complementary to [$^{131}$I]MIBG in terms of radiobiological properties and clinical indications.

absorbed dose from the alpha particle emitter Astatine-211 ($^{211}$At) to that from Yttrium-90 has been estimated to be 9 and 33 for 1,000 and 200 μm diameter tumors, respectively. Thus, alpha particles would be more appropriate for the treatment of smaller tumors (11–13). The development of a targeted radiotherapeutic approach that would selectively destroy these isolated cell clusters has the potential to dramatically improve durable response rates and outcomes.

There has been considerable interest in α-particle emitting radiopharmaceuticals due to the favorable radiobiologic properties of dense ionization of the tissues they enter, resulting in double-strand DNA breaks that is independent of free radical formation over much shorter path lengths (tens of microns) resulting in targeted cytotoxicity and lower off-target damage (14, 15). In addition to the long path lengths of β-particle radionuclides, $^{131}$I has the disadvantage of relatively lower linear energy transfer (LET) and generation of hydroxyl free radicals as a mechanism for DNA damage, causing upregulation of superoxide dismutase and resistance to radiotherapy (11, 14, 16).

Despite the clear promise of alpha radionuclide therapy, there are several issues with alpha particle therapy. One of the most important is the short half-life of 7.2 hours for $^{211}$At which limits long distance usage and shipment. In addition, in studies of long-lived alpha emitters, daughter isotopes can lead to toxic effects. However, with the straightforward decay scheme of $^{211}$At, this is unlikely to be a serious problem. Alpha particles are dangerous if inhaled, ingested, or absorbed through a wound but have no significant external exposure hazard. When they do interact with biological material, they are very damaging because of their relatively large mass and double charge. Specific targeting, rapid clearance from normal tissues, and minimization of retention of radiopharmaceuticals in healthy nontargeted tissues is of utmost importance.

$^{211}$At is a short-lived (7.2 hours half-life) α emitter and is an attractive radiotherapeutic due to the absence of long-lived α-emitting daughters and has considerably more potency and focused cytotoxicity than $^{131}$I (17, 18). Both $^{211}$At and $^{131}$I are radiohalogens, hence similar radiochemical strategies can be used to conjugate these isotopes onto a benzylguanidine moiety (13, 19–21). Meta-[$^{211}$At]astatobenzylguanidine ([$^{211}$At]MABG) demonstrates similar physicochemical properties to [$^{131}$I]MIBG, and shows NET-specific uptake into neuroblastoma cells *in vitro* (22).

[$^{211}$At]MABG showed potent antitumor effect in preclinical studies with malignant pheochromocytoma and neuroblastoma (17, 21, 23).

**Table 1.** Human neuroblastoma cell line and PDX models with relevant genomic data.

| Cell line or PDX | MYCN status | *ALK* mutation status | *TP53* mutation status |
|---|---|---|---|
| COG-N-415 | Amplified | F1174L | Wild type |
| COG-N-421x | Amplified | Wild type | Wild type |
| COG-N-424 | Amplified | Wild type | Wild type |
| COG-N-440 | Amplified | Wild type | Wild type |
| COG-N-452, COG-N-453[a] | Amplified | F1174L | Wild type |
| COG-N-471nb | Amplified | Wild type | Wild type |
| FELIX (COG-N-426) | Nonamplified | F1245C | Wild type |
| IMR-05 | Amplified | Wild type | Wild type |
| NB-1691 | Amplified | Wild type | Wild type |
| NLF | Amplified | Wild type | V203M |
| SK-N-BE(2) | Amplified | Wild type | C135F |
| SK-N-BE(2)-C | Amplified | Wild type | C135F |
| SK-N-SH | Nonamplified | F1174L | Wild type |

[a]Two models derived from the same patient.

The cytotoxicity of [$^{211}$At]MABG expressed as bound atoms/cell was nearly 1,400 times higher than [$^{131}$I]MIBG in SK-N-SH neuroblastoma cell lines (24). Finally, mAbs labeled with $^{211}$At demonstrated antitumor activity with limited toxicity in phase I clinical trials (25, 26). Together, these data supported the preclinical work here that further develops [$^{211}$At]MABG for high-risk neuroblastoma.

## Materials and Methods

### Cell culture

Human-derived neuroblastoma cell lines (**Table 1**) were obtained from the Children's Hospital of Philadelphia cell line bank, the Children's Oncology Group, or ATCC and were cultured in RPMI-1640 medium (Invitrogen) containing 10% FBS (Hyclone), 2 mmol/L L-Glutamine, and 1% streptomycin/penicillin at 37°C under 5% $CO_2$. Cells tested negative for *Mycoplasma* contamination and were authenticated by a short tandem repeat profile using the AmpFISTR Identifier kit (Applied Biosystems).

### NET overexpression and GFP-luciferase expression

To recapitulate human neuroblastoma and to obtain isogenic cell line pairs with NET overexpression, we initially used retroviral NET transduction to generate SK-N-BE(2)$^{NET}$, NLF$^{NET}$, and IMR-05$^{NET}$ cell lines and subsequently for sustained and optimized transduction we used a lentiviral construct expressing NET, GFP, and firefly luciferase to infect native neuroblastoma cell lines to generate isogenic cell line pairs NB1691$^{NET/GFP/LUC}$, IMR-05$^{NET/GFP/LUC}$, and SK-N-SH$^{NET/GFP/LUC}$ as described previously (27, 28). Of note, GFP was used for confirming efficiency of infection and not used for fluorescence imaging.

### RT-PCR

cDNA synthesis and RT-PCR was performed with Applied Biosystem's (ABI) High Capacity Reverse Transcription Kit as described previously. Commercial TaqMan probe and primer sets for *NET* (Assay ID: Hs01567441_m1), *GAPDH* (Assay ID: Hs99999905_m1) were purchased from ABI. Ratios of mRNA quantities were normalized by comparing mRNA expression of interest with the geomean of

mean *UBC*, *HPRT1*, and *GAPDH* expression. SK-N-BE (2)-C (ECACC, catalog no. 95011817, RRID:CVCL_0529) was used as a positive control and demonstrated that *NET* expression levels in the cell lines were within the linear range of the standard curve. All samples were tested in triplicate, and the result reported is the mean of three separate experiments.

### Immunoblots

Whole-cell protein was extracted with lysis buffer [Cell Signaling Technology Cell Lysis Buffer (10×), catalog no. 9803] containing protease and phosphatase inhibitor (Thermo Fisher Scientific, catalog no. 78440). Protein concentration was determined using the BCA protein assay (Pierce, catalog no. 23225). Approximately 0.02–0.04 mg of protein was resolved by SDS-PAGE and blotted as described previously (29) with hNET antibody (MAb Technologies, catalog no. NET17-1, RRID:AB_2921285) and Ku80 (Cell Signaling Technology, catalog no. 2753, RRID:AB_2257526) primary antibodies.

### IHC and tissue microarray staining

Tumors excised from mice were fixed with 10% buffered formalin phosphate (Thermo Fisher Scientific), paraffin embedded, and sectioned for staining with the hNET antibody (NET17-1 antibody, MAb Technologies, catalog no. NET17-1, RRID:AB_2921285) as described previously (3). NET17-1 antibody was used to stain a tissue microarray containing 34 neuroblastoma patient-derived xenograft (PDX) models and nine normal control tissues. Staining was performed on a Bond RXm automated staining system (Leica Biosystems). NET17-1 antibody was used at 1:500 dilution and antigen retrieval was performed with E1 retrieval solution (Leica Biosystems) for 20 minutes. Stained slides were then digitally scanned at 20× magnification on an Aperio CS-O slide scanner (Leica Biosystems). Image analysis was performed using Qupath open source software (30). Cytoplasmic staining intensity (0–3) was multiplied by percentage of positive cells to calculate an H-Score. The H-score was averaged between two cores from two different tumors for each tumor model.

### Radiosynthesis of [$^{125}$I]MIBG [$^{131}$I]MIBG and [$^{211}$At]MABG

$^{211}$At was produced on a JSW BC3015 Cyclotron at the University of Pennsylvania via the 209Bi($\alpha$,2n)$^{211}$At nuclear reaction using a solid bismuth (Bi) target irradiated at a 90° beam incidence angle. The beam energy was degraded from 30 to 28.3 MeV using a 75 μm aluminum degrader foil to avoid coproduction of 210At. The beam current was 5–10 μA depending on the requirement for the production. Radionuclidic purity was assessed by gamma and alpha spectroscopy on an Ortec GEM10P4-70 High-Purity Germanium Detector and Ortec ULTRA alpha spectrometer using Maestro Version 7 software operated on Windows 10. 2.

$^{211}$At was produced with total yields ranging from 37–370 MBq (1–10 mCi) with optimized distillation yields of 70%. Radionuclidic purity was greater than 99.9% with <0.01% $^{210}$At isotopic impurity. Iodine-125 (molar activity 80.3 GBq/μmole (2,170 mCi/μmole) and Iodine-131 (theoretical Molar Activity 603 GBq/μmole or 16,300 mCi/μmole) were purchased from Perkin Elmer and Nuclear Diagnostic Products Radiopharmacy, respectively. Radiosynthesis of [$^{125}$I]MIBG, [$^{131}$I]MIBG, and [$^{211}$At]MABG was performed using the previously described kit method (20). Briefly, [$^{211}$At]MABG was synthesized by electrophilic aromatic destannylation of polymer-bound tin leaving group. Resin-supported MBG precursor was used for [$^{131}$I]MIBG, [$^{125}$I]MIBG, and [$^{211}$At]MABG production as described in the package insert (31). Resin was provided by Progenics Pharmaceuticals, Inc., a Lantheus company. Up to 111 MBq (3 mCi) of [$^{211}$At]MABG with >95% radiochemical purity as determined by high-performance liquid chromatography was produced for the experiments described here.

### SPECT/CT studies

SPECT/CT fused images were acquired as maximum intensity projections of the gamma emissions obtained 24 hours after injection of 18.5 MBq (0.5 mCi) [$^{125}$I]MIBG in both IMR-05 and NB1691$^{NET/GFP/LUC}$ xenograft bearing CB17SC *scid*$^{-/-}$ mice using the Bioscan NanoSPECT 4-head SPECT/CT device equipped with tungsten-based multiplexing multipinhole collimators dedicated for small animal imaging. While imaging $^{211}$At is technically feasible, it generally does not yield useful or helpful images beyond a proof of concept given the low abundance and very low-energy photon emissions.

### [$^{131}$I]MIBG and [$^{211}$At]MABG cellular uptake studies in human-derived neuroblastoma cell lines

Increased NET expression on the surface of neuroblastoma tumors is well described and responsible for the active receptor-mediated uptake of MIBG (3, 4). Radiotracer internalization studies were performed in NET transfected cell lines and native cell lines to show dependency of the tumor uptake of both radionuclides on NET transporter expression using [$^{131}$I]MIBG or [$^{211}$At]MABG as described previously (32).

### Cell viability assays

Cell viability studies were performed as previously described with modifications (33). Briefly, cells were seeded at a density of 5,000 cells per well and 24 hours later solutions of [$^{211}$At]MABG or [$^{131}$I]MIBG were added at varying concentrations in quadruplicate. Cells were then assayed for viability at 72 hours using CellTiter Glo (Promega) and the luminescent signal was read on a Perkin Elmer Enspire Multi-Mode plate reader. Percent survival was calculated by dividing the treated wells by the control wells and multiplied by 100. Next, percent survival was graphed as a function of dose using a nonlinear sigmoidal dose–response curve (Graph Pad Prism for macOS Version 9.1.2) and effective doses for 50% reduction in cell viability were calculated.

### Institutional protocols for animal studies

All animal studies were approved by the Children's Hospital of Philadelphia Institutional Animal Care and Use Committee protocol (IACUC 000643). C.B-*Igh-1*$^{b}$/IcrTac-*Prkdc*$^{scid}$ (CB17SC *scid*$^{-/-}$; RRID: IMSR_TAC:cb17sc) mice used in the study were purchased from Taconic Biosciences and NOD.Cg-*Prkdc*$^{scid}$ *Il2rg*$^{tm1Wjl}$/SzJ (NSG; RRID:IMSR_JAX:005557) mice were acquired from Charles River. Both CB17SC *scid*$^{-/-}$ and NSG mice were bred and housed in the Department of Veterinary Research, Children's Hospital of Philadelphia. Strict isolation and testing for infectious agents as well as genetic standardization for the colonies was performed per IACUC protocols.

### Biodistribution studies

SK-N-SH$^{NET/GFP/LUC}$ transfected xenografts were enrolled at a tumor size of 0.2–0.3 cm$^3$. A total of 15 mice in each arm were injected intravenously via tail vein with [$^{131}$I]MIBG, [$^{211}$At]MABG, [$^{125}$I]MIBG, or sodium $^{211}$At-astatide, respectively, to assess for biodistribution at 30 minutes, 4 hours, and 24 hours after injection ($N = 5$ mice/timepoint). A fixed activity of 0.185 MBq (0.005 mCi) was used for each of these radionuclides. The total mass injected for the radionuclides is expected to be near the theoretical molar activity, although mass was not directly assessed. Parental SK-N-SH xenografts were also injected in a similar fashion with [$^{211}$At]MABG alone. Tracer dosing

and methodology were as described previously (24). Mice were euthanized at 30 minutes, 4 hours, and 24 hours after injection and dissected ($N = 5$ at each timepoint). Blood, organ, and tumor activity of either $^{131}$I or $^{211}$At was measured at each timepoint using a high efficiency gamma counter (2480 WIZARD$^2$, Perkin Elmer). Tissues measured included heart, muscle, lung, kidney, spleen, liver, skin, brain, bone, thyroid, small and large intestine, stomach, and tail. The percentage of the injected dose (%ID) per gram of tissue (ID/g) as well as per organ was calculated after appropriate decay correction was applied. Of note, with astatine decay, there is an emission of polonium K x-rays (as a consequence of its electron capture branch) and these have energies between 77 and 92 keV. These emissions are used for monitoring of $^{211}$At using the gamma counter. Clinical dose estimates were based on the assumption that the percent of administered activity in a particular organ adjusted for the relative fractional organ mass is the same in mice and humans. Residence times (cumulated activity divided by administered activity) were estimated and used as input data for the FDA-approved OLINDA/EXM software application to calculate absorbed doses for more than 20 normal organs (34).

### Toxicity studies

Radiotoxicity of intravenous $^{211}$At had been previously evaluated in immune competent B6C3F1 mice followed for 1 year with an LD10 of 0.551 MBq (equivalent to 28.1 MBq/kg; 0.76 mCi/kg; ref. 35). To establish the MTD of [$^{211}$At]MABG in CB17SC *scid*$^{-/-}$ mice, we tested four doses administered intravenously which were 16.28, 42.18, 81.77, and 163.91 MBq/kg (0.44, 1.14, 2.21, and 4.43 mCi/kg) in 10 mice per dose level and observed mice for at least 150 days. The broad range was chosen because the limits of toxicity for this species had not been defined in the literature. For longitudinal organ toxicity evaluation in CB17SC *scid*$^{-/-}$ mice, we initially explored doses of 16.3 and 41.5 MBq/kg (0.44 and 1.12 mCi/kg, respectively) of [$^{211}$At]MABG injected intravenously in 10 mice, based on a dose-escalation strategy. These two doses were chosen for the long-term study because the doses above 74 MBq/kg (2 mCi/kg) were not tolerated. Animals were monitored for a maximum of 6 months or until death or euthanized when they lost >20% weight or exhibited other signs of distress. Before therapy, at approximately 3 weekly intervals after therapy (until parameters returned to baseline levels) and at the time of sacrifice, blood was drawn from the retrorobital vein for hematologic parameters and renal and hepatic chemistry. After sacrifice, kidney, intestine, lung, and bone marrow were fixed and underwent histopathologic evaluation.

Once we had established that these intravenous doses were well tolerated, we gradually dose-escalated to a maximum tolerated dose (MTD) of 66.7 MBq/kg (1.8 mCi/kg) in CB17SC *scid*$^{-/-}$ and 51.8 MBq/kg (1.4 mCi/kg) in NSG mice ($n = 10$ each) administered intraperitoneally. Mice were monitored by biweekly weights and daily for any signs of distress. After validating that intraperitoneal and intravenous administration of [$^{211}$At]MABG have comparable distribution and kinetics (data not shown), consistent with prior observations with [$^{131}$I]MIBG (36). Intraperitroneal dosing was used for all efficacy studies. [$^{131}$I]MIBG dosing was extrapolated from clinical experience [666 MBq/kg (18 mCi/kg)] and an MTD was established in mice based on tolerability.

### Efficacy studies in xenografted murine models

Efficacy studies were designed to assess the antitumor activity of [$^{211}$At]MABG compared with [$^{131}$I]MIBG and placebo. PDX models (**Table 1**) were generated as described previously in the NCI Pediatric Preclinical in Vivo Testing (PIVOT) Program (37, 38). PDX models were established in the laboratory of Dr. C. Patrick Reynolds and obtained through the Children's Oncology Group Cell Culture and Xenograft Repository. Briefly, viably cryopreserved neuroblastoma tumor fragments or blood obtained at postmortem from patients with progressive relapsed disease (COG-N-453x and Felix, respectively) were engrafted subcutaneously into the flanks of C.B-Igh-1b/IcrTac-Prkdcscid mice (Taconic Farms), and passaged once tumors reached 200 mm$^3$. Cell-derived xenografts (CDX) were generated by subcutaneously inoculating 10 million SK-N-SH$^{NET/GFP/LUC}$ cells suspended in Matrigel (Corning catalog no. 354248) into the flank of CB17SC *scid*$^{-/-}$ female mice and passaged at least once. Tumor fragments were then engrafted into study mice for experimental trials.

Once tumors reached roughly 0.2–0.3 cm$^3$, mice were randomized into treatment groups to receive treatments at the indicated regimen (MTD bolus or fractionated dosing). Fractionated dosing regimen was used to decrease normal tissue toxicity while maximizing antitumor efficacy as described previously. In the CDX SK-N-SH$^{NET/GFP/LUC}$ model, two doses of 51.8 and 66.7 MBq/kg (1.4 and 1.8 mCi/kg, respectively) of [$^{211}$At]MABG were given to understand whether dose intensity correlated with response. Treatment arms for the CDX model (SK-N-SH$^{NET/GFP/LUC}$) included (i) Vehicle; (ii) [$^{211}$At]MABG bolus at 51.8 MBq/kg (1.4 mCi/kg); (iii) [$^{211}$At]MABG bolus at 66.7 MBq/kg (1.8 mCi/kg); and (iv) [$^{131}$I]MIBG bolus at 666 MBq/kg (18 mCi/kg). Felix and COG-N-453x PDX models were randomized to the following arms: (i) Vehicle; (ii) [$^{211}$At]MABG bolus at 66.7 MBq/kg (1.8 mCi/kg); (iii) Fractionated doses of [$^{211}$At]MABG at 16.6 MBq/kg/fraction (0.45 mCi/kg) × 4 over 11 days; and (iv) [$^{131}$I]MIBG bolus at 666 MBq/kg (18 mCi/kg). Potassium iodide (SSKI) was given intraperitoneal for thyroid protection (1 mg/kg potassium iodide in a volume of 0.10 mL/g) the day prior to treatment, 30 minutes prior to the radioactive injection and daily for one day after treatment for [$^{211}$At]MABG or 7 days after [$^{131}$I]MIBG therapy (6).

Mice were monitored for body weight and distress for a maximum of 60 days or until the tumor burden endpoint of 3 cm$^3$ was reached. Tumor volumes were measured weekly using calipers, and were calculated as: volume = $(\pi/6)$(diameter$^3$), as described previously (39).

Disseminated neuroblastoma models were established in NSG mice by intravenous tail vein injection of $1 \times 10^6$ IMR-05$^{NET/GFP/LUC}$ cells. A pilot study was performed to follow tumor formation and dissemination using bioluminescence imaging (BLI). Mice in the treatment arm ($n = 19$) were treated with [$^{211}$At]MABG intraperitoneally with four fractionated doses using 12.95 MBq/fraction (0.35 mCi//kg/fraction; in 500 μL diluent each) given over 11 days. Therapy was initated on day 5 after injection of neuroblastoma cells before BLI showed detectable activity (based on our pilot temporal tumor progression experiments). Control mice ($n = 10$) were given placebo (500 μL of saline) at each of the above timepoints. Thyroid protection with SSKI was administered as described previously. Tumor cell dissemination was monitored biweekly until day 60 and then switched to weekly monitoring performed till 150 days or attainment of toxicity endpoints. Mice were monitored for toxicity and sacrificed per protocol if noted to have severe weight loss or distress.

### BLI and analysis

Images were acquired using the IVIS Spectrum C. D-luciferin (VivoGlo Luciferin, In Vivo Grade, Promega) was injected intraperitoneally into mice at 150 mg/kg 10 minutes prior to BLI. Animals were then anesthetized using 2% isoflurane and placed into the imaging chamber. For two-dimenisonal BLI, the system was set to acquire images without any emission filter (open) to maximize sensitivity and to improve detection limit with autoexposure. BLI analysis was done

using Living Image 4.4 software. Quantification used only the total photon flux (photons per second) and did not depend on exposure time.

### Statistical methods

Linear mixed-effects model was used to test the difference in the rate of tumor volume changing over time between different groups. Tumor volume was first square root transformed before modeling due its skewed distribution. The model included group, day, and group-by-day interaction as fixed effects, and included a random intercept and a random slope for each mouse. A significant group-by-day interaction suggests that the tumor volume changes at different rates for the two comparison groups. The model used the control group as the reference group and created separate group indicators and interaction terms for other groups. Piecewise linear mixed-effects model was used to test the difference in the rate of body weight changing over time between difference groups. The piecewise model assumes one slope before day 7 and another slope after day 7. An overall test of difference in any slopes between the groups was used to test for group difference in the weight change over time. Survival curves were estimated using Kaplan–Meier method and compared between groups using log-rank test. These analyses were performed in SAS 9.3.

The rest of data were analyzed using the Graph Pad Prism (Prism 9 for macOS Version 9.1.2 GraphPad Software, www.graphpad.com; GraphPad Prism, RRID:SCR_002798). Unless otherwise noted, data were summarized using the mean (±SEM) and compared between groups using two-sample *t* test. BLI analysis was done using Living Image 4.4 software. Quantification used only the total photon flux (photons per second). In all analyses, a $P$ value <0.05 is considered statistically significant.

### Data availability

The data generated in this study are available upon request from the corresponding author.

**Table 2.** Extrapolated human dosimetry (MIRD) for [$^{131}$I]MIBG and [$^{211}$At]MABG from biodistribution studies using the FDA-approved OLINDA/EXM application.

| | Gy/175 mCi ([$^{131}$ I]MIBG) | Gy/2 mCi ([$^{211}$At]MABG) |
|---|---|---|
| Adrenals | 0.457 | 0 |
| Brain | 0.139 | 0.427 |
| Breasts | 0.186 | 0 |
| Gallbladder wall | 0.858 | 0 |
| Large intestine wall (lower) | 0.471 | 0 |
| Small intestine | 9.12 | 0.009 |
| Stomach wall | 2.74 | 0.007 |
| Large intestine wall (upper) | 17 | 0.016 |
| Heart wall | 1.82 | 2.401 |
| Kidneys | 2.05 | 2.355 |
| Liver | 2.98 | 3.368 |
| Lungs | 0.834 | 1.343 |
| Muscle | 1.94 | 2.856 |
| Ovaries | 0.766 | 0 |
| Pancreas | 0.662 | 0 |
| Red marrow | 2.46 | 4.459 |
| Osteogenic cells | 2.8 | 20.155 |
| Skin | 0.144 | 0 |
| Spleen | 17.6 | 2.264 |
| Testes | 0.158 | 0 |
| Thymus | 0.323 | 0 |
| Thyroid | 342 | 41.174 |
| Urinary bladder wall | 0.29 | 0 |
| Uterus | 0.652 | 0 |
| Total body | 0.858 | 0.622 |
| EDE | 13.9 | 0.419 |
| ED | 18.5 | 3.169 |

Abbreviations: ED, equivalent dose; EDE, effective equivalent dose; Gy, gray; MIRD, medical internal radiation dose.

## Results

### Preclinical models, biodistribution, toxicity, and dose-finding studies

Cell line models of human neuroblastoma show low expression of *SLCA6* (NET) mRNA and protein compared with human primary neuroblastomas and PDX models (**Fig. 1A–C**). Human tumor PDX array showed overall very high differential NET expression (Supplementary Fig. S1). We therefore overexpressed human *SLC6A* in five neuroblastoma cell lines to recapitulate expression levels observed in patient samples (**Fig. 1A** and **B**). NET transfected lines showed higher internalization of [$^{131}$I]MIBG and [$^{211}$At]MABG compared with the respective parental lines, and competitive inhibition using desipramine showed the specificity of this forced overexpression (**Fig. 1D** and **E**). Scintigraphy with SPECT fused imaging confirmed tumor-specific localization of radiolabelled NET ligands (**Fig. 1F**).

Here we performed uptake studies after injection of [$^{211}$At]MABG, [$^{131}$I]MIBG, [$^{125}$I]MIBG, and free sodium astatide in CB17SC *scid*$^{-/-}$ mice bearing 0.2 cm$^3$ flank xenograft tumors followed by quantification of activity in harvested tumor and vital organs (Supplementary Fig. S2). There was significant accumulation and retention of both [$^{211}$At]MABG and [$^{131}$I]MIBG in the tumors at 4 and 24 hours. There was also marked accumulation of activity from [$^{211}$At]MABG in the thyroid and stomach, presumably as free astatide. In general, the biodistribution of [$^{211}$At]MABG largely mirrored that of [$^{131}$I]MIBG in the 24-hour time period studied here. These studies were descriptive in nature and not powered for statistical analysis. We used these data to extrapolate estimated human absorbed dose values shown in **Table 2**.

[$^{211}$At]MABG doses above 74 MBq/kg (2 mCi/kg) caused >20% weight loss or death, establishing 66.7 MBq/kg (1.8 mCi/kg) as the MTD in CB-17SC *scid*$^{-/-}$ mice. Longitudinal toxicity studies showed intravenous [$^{211}$At]MABG to be well tolerated in non–tumor-bearing CB17SC *scid*$^{-/-}$ mice at doses of 16.3 and 41.5 MBq/kg (0.44 and 1.12 mCi/kg) except for transient thrombocytopenia with a nadir at 6 weeks (**Fig. 2A**; $P = 0.0023$ and $P = 0.0002$, respectively). There was no organ toxicity on histopathologic review of liver, kidney, skin, muscle, stomach, large and small intestine, spleen, lung, heart, thyroid, brain, and femur at either dose, and no biochemical evidence of thyroid or other organ toxicity (Supplementary Fig. S3). Both bolus 66.7 MBq/kg (1.8 mCi/kg) and fractionated dosing 16.6 MBq/kg/fraction (0.45 mCi/kg) × 4 over 11 days) of [$^{211}$At]MABG caused transient weight loss (**Fig. 2B**), similar to bolus [$^{131}$I]MIBG administration in CB-17SC *scid*$^{-/-}$ mice (data not shown). NSG mice tolerated fractionated dosing [$^{211}$At]MABG with a MTD of 12.9 MBq/kg/fraction (0.35 mCi/kg) × 4 doses over 11 days (data not shown).

### Efficacy of [$^{211}$At]MABG in preclinical models of neuroblastoma

[$^{211}$At]MABG showed potent cytotoxicity across a panel of 10 neuroblastoma cell lines, and in each case it was significantly more

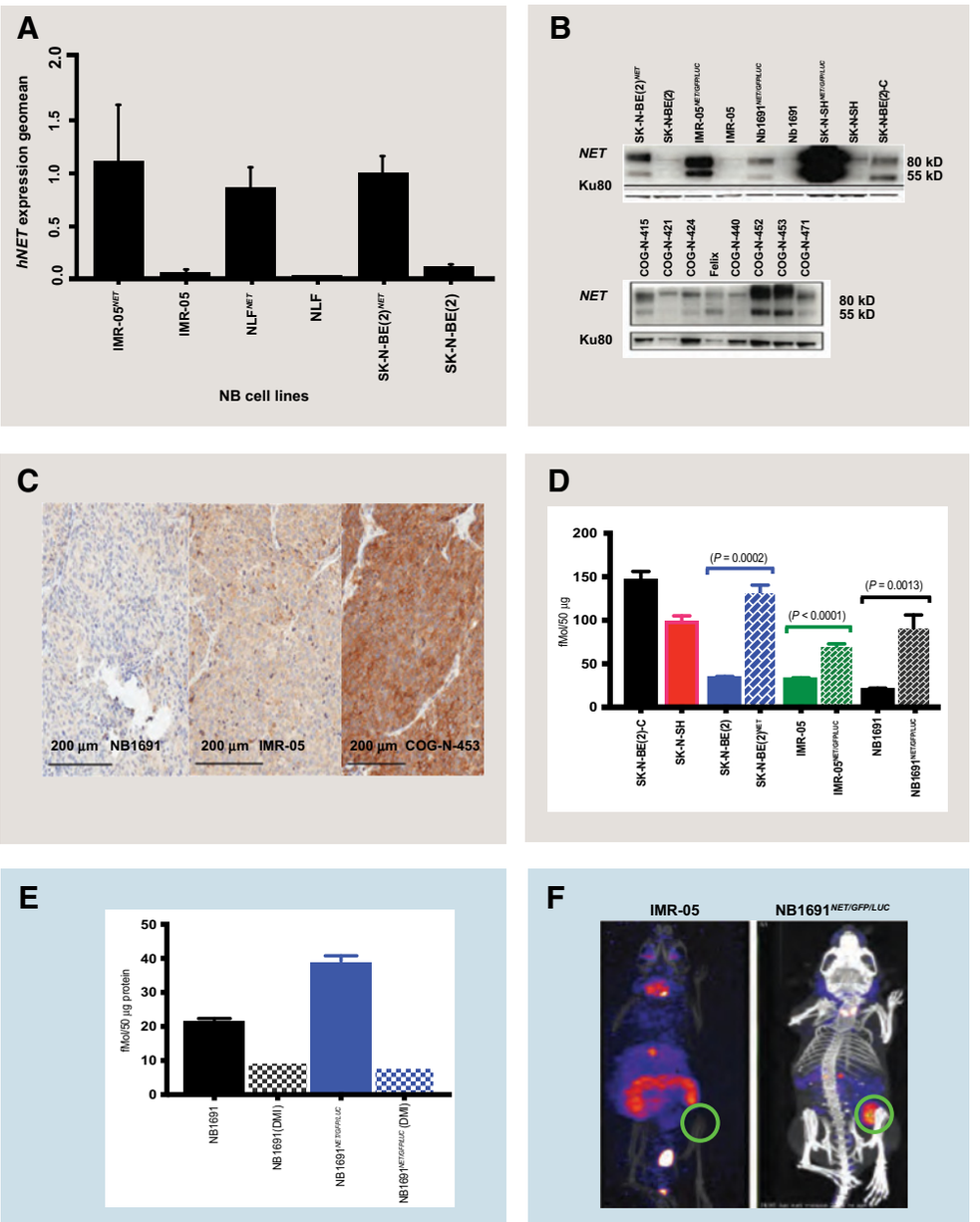


**Figure 1.**

NET expression and NET-targeting radiotherapeutic uptake in neuroblastoma cell lines. **A,** RT-PCR of *SLC6A* (NET) expression in parental neuroblastoma cell lines and genetically modulated NET isogenic pairs. The geometric mean of *SLC6A* expression is normalized to housekeeping genes *HPRT*, *TBP*, and *UBC*. **B,** NET immunoblot for parental, isogenic cell lines and PDX models. Two separate bands are observed with the glycosylated form at 80 kD, and nonglycosylated band at 55 kD. **C,** NET IHC in neuroblastoma xenografts, NB1691, IMR-05, and COG-N-453x, showing that PDX models retain high expression. **D,** [$^{131}$I]MIBG shows increased internalization in NET transfected cells compared with parental cells, mirroring NET expression as defined by RT-PCR. Differences in internalization between isogenic cell pairs was statistically significant. SK-N-BE(2)$^{NET}$ versus SK-N-BE (2) ($P = 0.0002$); IMR-05$^{NET}$ versus IMR-05 ($P < 0.0001$); NB1691$^{NET/GFP/LUC}$ versus NB1691 ($P = 0.0013$). **E,** [$^{211}$At]MABG uptake in NB1691 cells with and without NET overexpression, with specificity demonstrated by desipramine blockade. **F,** SPECT/CT images obtained 24 hours after injection of 16.65 MBq (0.5 mCi) of [$^{125}$I]MIBG showing localization in the high NET-expressing lentiviral transfected NB1691$^{NET/GFP/LUC}$ xenografts (right) as opposed to parental IMR-05 xenografts (left). Area of xenograft marked with green circles. Nonspecific bowel uptake is observed in the IMR-05 model.

cytotoxic than [$^{131}$I]MIBG (**Fig. 2C**). Higher $EC_{50}$ values were obtained for NB1691$^{NET/GFP/LUC}$, SK-N-BE(2)$^{NET}$, and SK-N-BE (2)-C cell lines and notably each of these lines has a *TP53* mutation or *MDM2* amplification.

The efficacy and toxicity of both radiolabeled agents were studied in one CDX (SK-N-SH$^{NET/GFP/LUC}$ and two PDX (Felix and COG-N-453x) neuroblastoma models in a randomized controlled trial with 10 mice per arm (with the exception of $n = 5$ for the [$^{211}$At]MABG bolus

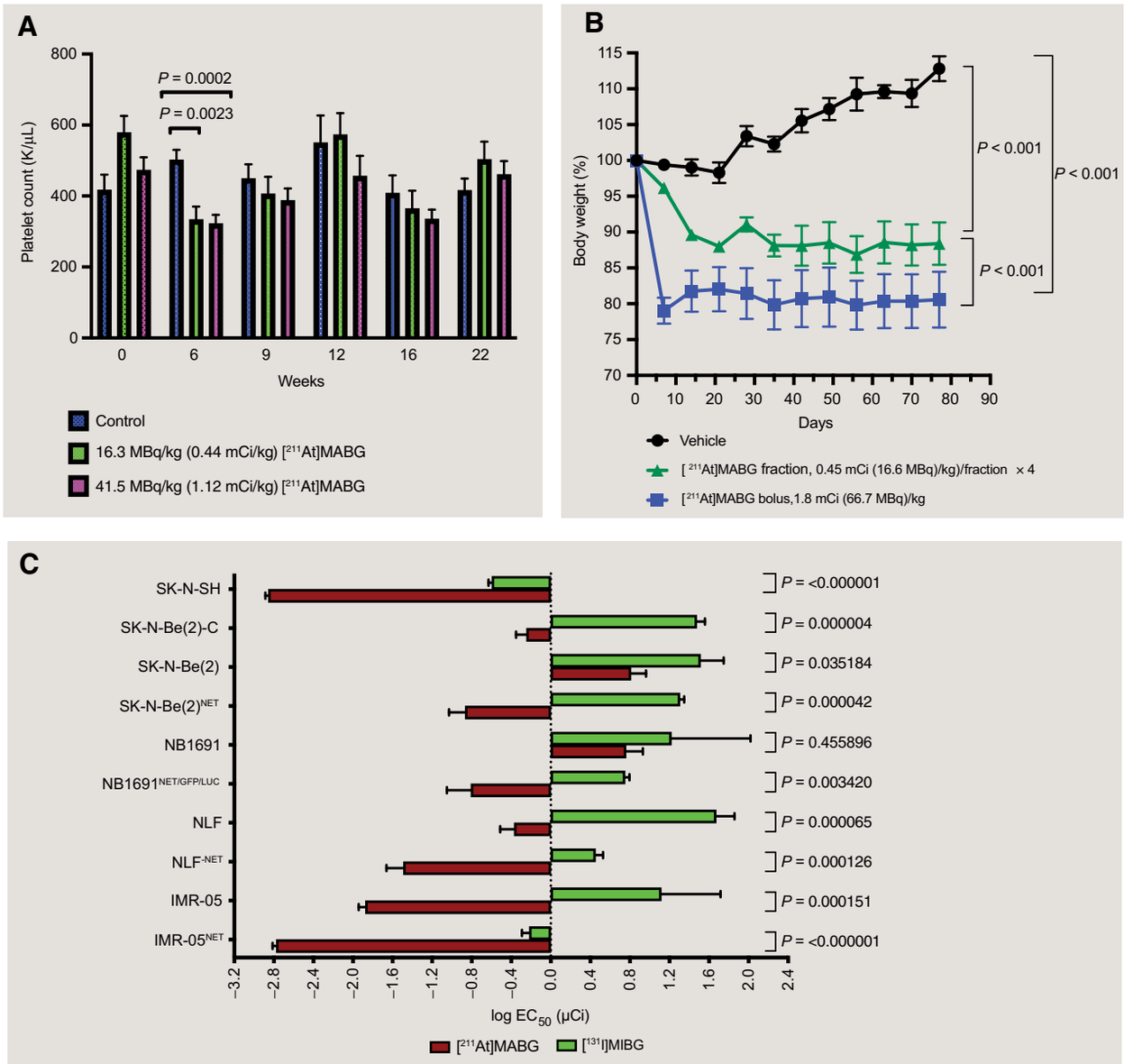


**Figure 2.**

Toxicity of [$^{211}$At]MABG in murine models. **A,** Effects of bolus [$^{211}$At]MABG injection on platelet counts. Nadir was noted at 6 weeks after administration of [$^{211}$At]MABG. No animal died of hematologic toxicity and recovery was noted in the counts in 3 weeks. **B,** Weight loss following after bolus dosing with [$^{211}$At]MABG is abrogated by a fractionated schedule. [$^{211}$At]MABG was administered as a bolus dose of 66.7 MBq/kg (1.8 mCi/kg) ($n = 10$) or in four fractions of 16.6 MBq/kg/fraction (0.45 mCi/kg) over 11 days ($N = 10$ mice). Using linear mixed-effects model, $P$ value for group comparison was as follows: (i) bolus versus vehicle, $P < 0.001$, (ii) fractionated versus vehicle, $P < 0.001$, (iii) bolus versus fractionation, $P < 0.001$. **C,** [$^{211}$At]MABG shows potent cytotoxicity across a panel of neuroblastoma cell lines. Cells were exposed to a 4-log dose range of [$^{131}$I]MIBG or [$^{211}$At]MABG. Both agents show differential cytotoxicity in human neuroblastoma cell models; increased cytotoxicity was seen with NET transfected lines compared with native lines. [$^{211}$At]MABG shows potent cytotoxicity in radioresistant cell lines such as SK-N-BE (2)-C and shows superior cytotoxicity in neuroblastoma cell lines compared with [$^{131}$I]MIBG.

arm in the Felix model). SK-N-SH was established at diagnosis and is *MYCN* nonamplified and *ALK* mutated (F1174L); COG-N-453x was established from postmortem blood draw and is *MYCN* amplified and *ALK* mutated (F1147L); Felix (COG-N-426x) was also established postmortem and is *MYCN* nonamplified and *ALK* mutated (F1245C). All three models are *TP53* wild type and show high NET expression.

The efficacy of [$^{211}$At]MABG was initially evaluated at both the MTD of 66.7 MBq/kg (1.8 mCi/kg) as well at a lower dose 51.8 MBq/kg (1.4 mCi/kg) and compared with [$^{131}$I]MIBG delivered at MTD dosing of 666 MBq/kg (18 mCi/kg) in the CDX SK-N-SH$^{Net/LUC/GFP}$ model (**Fig. 3A**). Tumor growth delay was not significantly different with either of the bolus [$^{211}$At]MABG doses delivered. There was higher treatment-related mortality rate in the [$^{131}$I]MIBG arm compared with the [$^{211}$At]MABG arm. Thereafter, the estabilised bolus [$^{211}$At]MABG dose of 66.7 MBq/kg (1.8 mCi/kg) was compared with a fractionated schedule [four fractions of 16.6 MBq/kg (0.45 mCi/kg) over 11 days]

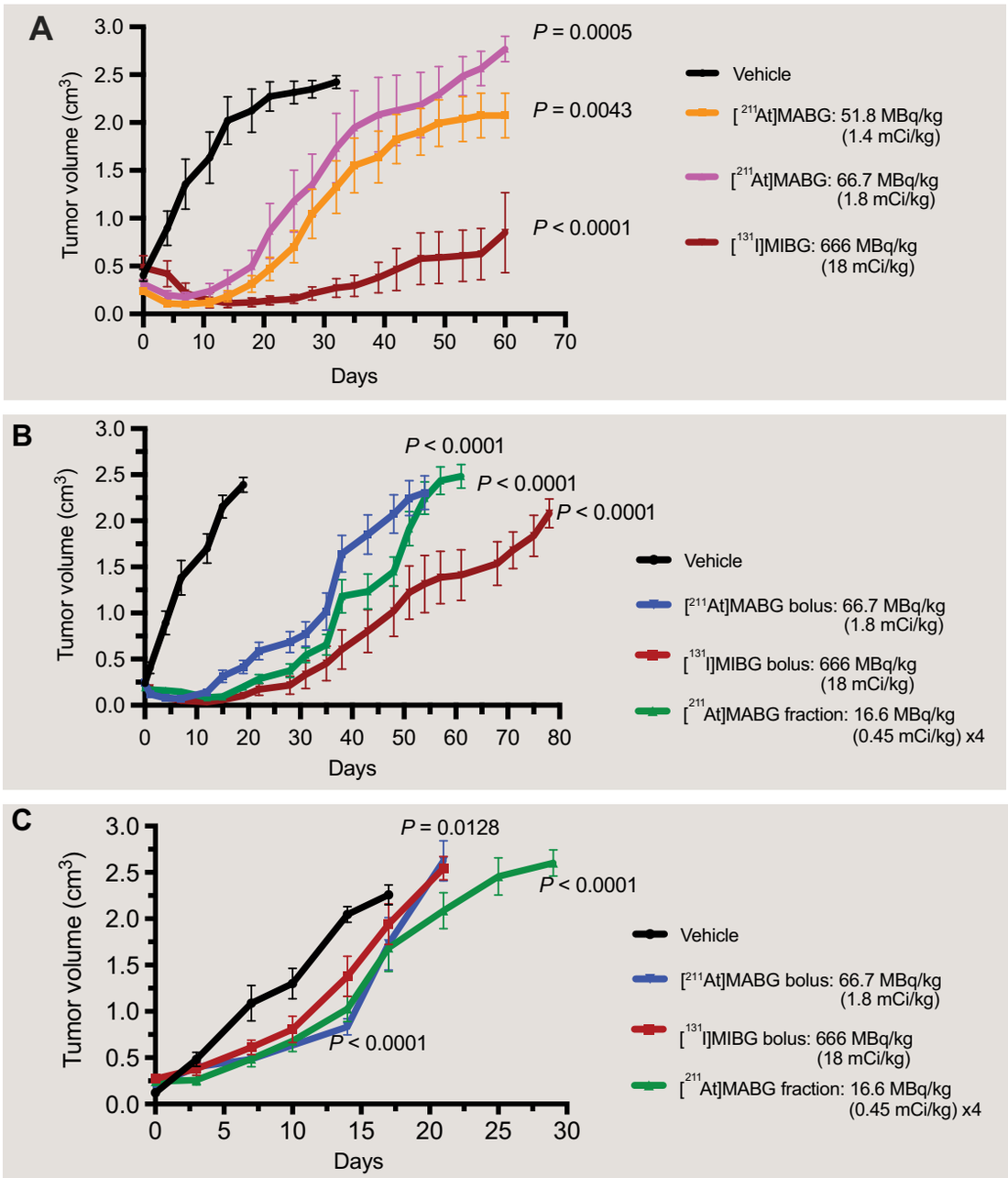


**Figure 3.**

[$^{211}$At]MABG shows efficacy in murine models of neuroblastoma. **A,** Mice bearing SK-N-SH$^{NET/GFP/LUC}$ xenografts (CDX) tumors of about 0.2 cm$^3$ in size at the time of enrollment were randomized ($n$ = 10/arm) to the following treatment arms administered intravenously: Vehicle, [$^{211}$At]MABG bolus at 51.8 MBq/kg (1.4 mCi/kg), [$^{211}$At]MABG bolus at 66.7 MBq/kg (1.8 mCi/kg), and [$^{131}$I]MIBG bolus at 18 mCi/kg (666 MBq/kg). **B,** Subsequently, the COG-N-453x (PDX) model was treated intraperitoneally with MTDs either as bolus dose 66.7 MBq/kg (1.8 mCi/kg) or 16.6 MBq/kg (0.45 mCi/kg) × 4 in equal fractionated doses of [$^{211}$At]MABG over 11 days or with [$^{131}$I]MIBG at 666 MBq/kg (18 mCi/kg). Linear mixed-effects analysis showed that there was a significant tumor growth delay in the COG-N-453x PDX models treated with [$^{211}$At]MABG fractionated doses ($n$ = 10) and [$^{211}$At]MABG ($n$ = 10) bolus doses when compared with the vehicle ($n$ = 10) group. [$^{131}$I]MIBG arm showed significant tumor growth delay in this model ($n$ = 10). **C,** In addition, Felix (PDX) model was treated with [$^{211}$At]MABG intraperitoneally at 66.7 MBq/kg (1.8 mCi/kg) given as a bolus or 16.6 MBq/kg (0.45 mCi/kg) × 4 fractionated doses over 11 days or with [$^{131}$I]MIBG at 666 MBq/kg (18 mCi/kg). Tumor growth delay was also seen in the Felix PDX model with both [$^{211}$At]MABG bolus ($n$ = 10) and fractionated dosing ($n$ = 5) and in the [$^{131}$I]MIBG treated arm ($n$ = 10) when compared with vehicle ($n$ = 10) arm.

and to bolus [$^{131}$I]MIBG dosing (666 MBq/kg;18 mCi/kg) in the two PDX models studied. In the SK-N-SH and COG-N-453x models, there was significant tumor regressions with both the bolus and fractionated dosing that were more durable with [$^{131}$I]MIBG (**Fig. 3A** and **B**), which is perhaps not unexpected due to the much longer half-life of $^{131}$I, but all tumors eventually regrew in all arms. There was minimal efficacy of

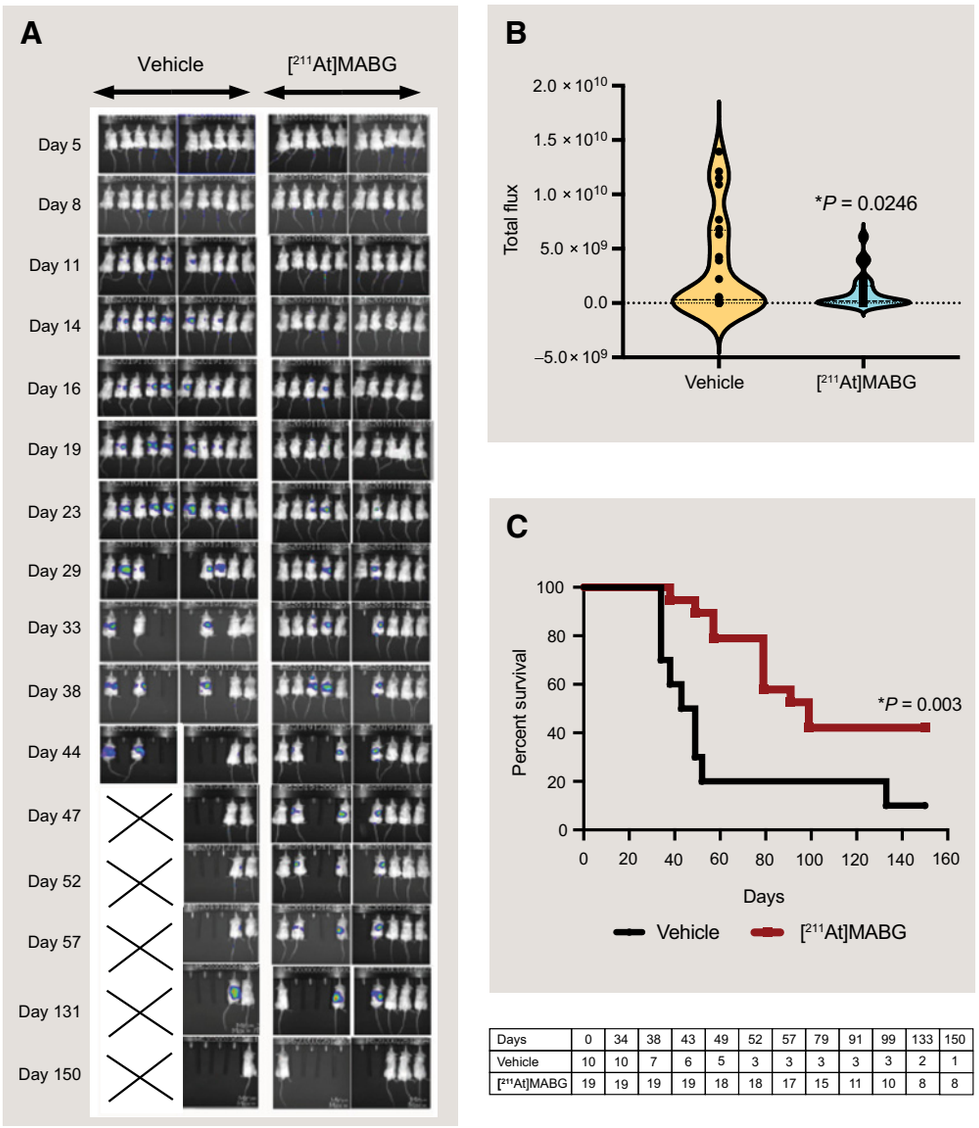


| Days | 0 | 34 | 38 | 43 | 49 | 52 | 57 | 79 | 91 | 99 | 133 | 150 |
|---|---|---|---|---|---|---|---|---|---|---|---|---|
| Vehicle | 10 | 10 | 7 | 6 | 5 | 3 | 3 | 3 | 3 | 3 | 2 | 1 |
| [211At]MABG | 19 | 19 | 19 | 19 | 18 | 18 | 17 | 15 | 11 | 10 | 8 | 8 |

**Figure 4.**

[$^{211}$At]MABG delays tumor progression in a minimal residual disease model of neuroblastoma. **A,** Bioluminescence images of NSG mice injected intravenously via tail vein with $1 \times 10^6$ IMR-05$^{NET/GFP/LUC}$ cells. Briefly, 1 million IMR-05$^{NET/GFP/LUC}$ neuroblastoma cells were injected via tail vein into NSG mice at day 0 and intraperitoneal injections of four fractionated doses of [$^{211}$At]MABG. 12.9 MBq/kg/fraction (0.35 mCi/kg) over 11 days were started from day 5 along with thyroid protective SSKI drops (1 mg/kg). Each column represents one mouse and each row represents timepoints, as indicated. Shown here are 10 mice from the vehicle group and only 10 representative mice (of $n = 19$) from [$^{211}$At]MABG treated group. Subsequent empty spaces represent mice that had reached tumor endpoint. **B,** Violin plots show the distribution of total flux (photons/second) integrated over the region of interest among vehicle ($n = 10$) and [$^{211}$At]MABG treated group ($n = 19$) during the course of these studies. Data analysis was done for all the mice enrolled in the vehicle ($n = 10$) and treated ($n = 19$) group even though only 10 representative mice in treatment are shown here. [$^{211}$At]MABG treated group shows decreased dissemination of tumor cells as compared with controls. **C,** Kaplan–Meier survival curve for vehicle and [$^{211}$At]MABG treated group is shown. Log-rank *P* value was 0.003. Survival estimates in the treated group at day 60 was 0.79 [95% confidence interval (CI), 0.53–0.92] versus 0.20 (95% CI, 0.03–0.47) in the vehicle group; at day 90 treated group was 0.58 (95% CI, 0.33–0.76) versus 0.2 (95% CI, 0.03–0.47) in the vehicle group and at day 150 treated group was 0.42 (95% CI, 0.20–0.62) versus 0.1 (95% CI, 0.01–0.36) in the vehicle group.

both targeted radiotherapies in the Felix model (**Fig. 3C**). Fractionated dosing appeared to be better tolerated in both PDX models.

We next studied the impact of [$^{211}$At]MABG on disseminated neuroblastoma using a tail vein tumor inoculation model in NSG mice to simulate microscopic minimal residual disease. Mice inoculated with 1 million IMR-05$^{NET/GFP/LUC}$ cells showed tumor engraftment, with BLI arising in the abdominal cavity within 12–15 days. Intervention trials with fractionated dosing began at day 5 after injection of tumor cells to mimic the clinical setting of isolated tumor cells or clumps in the metastatic niche, and based on pilot data on rate of engraftment. BLI in pilot studies show establishment of metastatic disseminated disease by day 7 after injection of tumor cells necessitating initiation of therapy by day 5 (Supplementary Fig. S4). Onset of disseminated disease was significantly delayed in the [$^{211}$At]MABG

treated animals (median 40.15 ± 11.5 days vs. 15 ± 16.4 days; and at day 60, 8 of 9 of the [$^{211}$At]MABG treated mice were alive as compared with 2 of 10 of the control mice (**Fig. 4A**). The total flux of photons, as analyzed by the IVIS software in the vehicle and treated group confirmed decreased spread of neuroblastoma cells in the treated group compared with the vehicle ($P = 0.0246$; **Fig. 4B**). A total of 42% of enrolled mice remained disease free and survived through the course of this experiment for more than 150 days (**Fig. 4C**), while only 1 mouse in the control group survived and presumably did not show tumor engraftment. Therapy was well tolerated except in one mouse in the treatment arm which experienced 20% weight loss and was euthanized. There were no other noticeable signs of toxicity.

## Discussion

Current cure rates for neuroblastoma remain mired at approximately 50% despite highly intensive multimodal therapies, thus more effective therapies are urgently needed. The currently available targeted radiotherapeutic [$^{131}$I]MIBG is a NET ligand that is rapidly internalized and has impressive single-agent activity in the relapsed and/or refractory setting (5, 7, 40–43), and is now being studied in newly diagnosed patients (NCT03126916). However, responses to [$^{131}$I]MIBG therapy are often transient due to reemergence of disease that likely was not targeted because of small metastatic clusters or single cells in the bone marrow compartment that would not sustain lethal DNA damage by the long pathlength beta particles emitted by $^{131}$I. This is the first study that we are aware of that attempts to address this issue with [$^{211}$At]MABG in a disseminated neuroblastoma xenotransplatation model.

Alpha particles have the potential to overcome this limitation due to short path lengths and high LET. Here we show that [$^{211}$At]MABG and [$^{131}$I]MIBG have very similar biodistribution patterns and concentration in neuroblastoma xenografts, confirming prior reports (24, 44). Previous studies have shown that a potential problem in delivering [$^{211}$At]MABG is the deastatination of $^{211}$At-labeled compounds due to the relatively low strength of the carbon-astatine bond (24, 45, 46). However, $^{211}$At has been shown to be safe in two clinical trials to date (25, 47). Results indicate no dose-limiting toxicities. On the basis of our biodistribution studies and toxicity studies, we predict that the radionuclide will be well tolerated because there was no concerning emesis, diarrhea, or significant weight loss noted in the mice treated with [$^{211}$At]MABG. The weight loss noted was transient with quick recovery to baseline. This is not surprising given the short path length of the alpha particle and the expected turnover of the gut mucosa. Most of the intraluminal alpha particles will irradiate only the mucus lining of the gut and those that do irradiate the underlying cells will likely have limited if any effect due to turnover. We also showed that [$^{211}$At]MABG is approximately 3 log more potent than [$^{131}$I]MIBG *in vitro*. Finally, we showed that [$^{211}$At]MABG has antitumor activity at least equivalent to [$^{131}$I]MIBG in the short term; longer term efficacy might be realized by repetitive dosing or by combination therapy with [$^{131}$I]MIBG. We also show that [$^{211}$At]MABG can prolong survival in a model that simulates microscopic disseminated disease. It must be emphasized that we are not seeking to show that [$^{211}$At]MABG is the superior radionuclide of the two, but to provide a complementary radionuclide to add to the existing gains noted with [$^{131}$I]MIBG in the relapsed/refractory setting. Taken together, these data support the development of [$^{211}$At]MABG as a complementary targeted radiotherapeutic for patients with high-risk neuroblastoma.

Much of the initial data with [$^{211}$At]MABG in this disease was generated well over a decade ago. Logistical difficulties precluded IND-enabling studies as very few cyclotrons are capable of producing $^{211}$At. However, there is now significant momentum and clinical proof of concept of the utility of alpha emitting radiotherapy for cancer (48–50). We plan to develop a phase I/IIb clinical trial in which patients with neuroblastoma will be first treated with four fractions of [$^{211}$At]MABG, followed by a combination of [$^{211}$At]MABG and [$^{131}$I]MIBG depending on the response to [$^{211}$At]MABG. Our work has shown the tolerance and efficacy of fractionated [$^{211}$At]MABG as opposed to a single administration and therefore we propose the usage of four fractions of [$^{211}$At]MABG and assessment of response. The clinical, radiological, and bone marrow response of fractionated [$^{211}$At]MABG will be integral in determining the tolerance and need for subsequent combinatorial [$^{211}$At]MABG and [$^{131}$I]MIBG. This will be an investigator initiated, single institution, phase I, dose-escalation trial of [$^{211}$At]MABG in relapsed or primary refractory neuroblastoma that is [$^{123}$I]MIBG avid. We plan to use the rolling six phase I trial design for the conduct of this study.

### Authors' Disclosures

V. Batra reports grants from U.S. Department of Defense, St. Baldrick's Fellowship Grant, ALSF REACH Grant, George L. Ohrstrom, Jr. Foundation, Hyundai Hope on wheels Scholar, and CCCR-ALSF Young Investigator Award during the conduct of the study. D.A. Pryma reports grants from Department of Defense during the conduct of the study; grants and personal fees from Siemens, 511 Pharma, Fusion pharmaceuticals, Lantheus, and Point; personal fees from Ipsen, Bayer, Curium, and Actinium; and grants from Nordic nanovector outside the submitted work; in addition, D.A. Pryma has a patent for At-211 PTT issued and licensed to Trevarx. J.M. Maris reports personal fees from Jubilant Radiopharma and Innervate Radiopharma during the conduct of the study. No disclosures were reported by the other authors.

### Authors' Contributions

**V. Batra:** Conceptualization, data curation, investigation, visualization, writing–original draft, writing–review and editing. **M. Samanta:** Conceptualization, data curation, investigation, visualization, writing–original draft, writing–review and editing. **M. Makvandi:** Conceptualization, data curation, investigation, visualization, writing–review and editing. **D. Groff:** Data curation, investigation. **P. Martorano:** Data curation, investigation. **J. Elias:** Data curation, investigation. **P. Ranieri:** Data curation, investigation. **M. Tsang:** Data curation, investigation. **C. Hou:** Data curation, investigation. **Y. Li:** Data curation, formal analysis. **B. Pawel:** Data curation, investigation, visualization. **D. Martinez:** Data curation, investigation, visualization. **G. Vaidyanathan:** Conceptualization. **S. Carlin:** Data curation, investigation. **D.A. Pryma:** Conceptualization, resources, supervision, funding acquisition, investigation, writing–original draft, project administration, writing–review and editing. **J.M. Maris:** Conceptualization, resources, supervision, funding acquisition, investigation, writing-original draft, project administration, writing–review and editing.

### Acknowledgments

This work was supported by NIH grants R35 CA220500 (J.M. Maris) and R01 219006 (D.A. Pryma), Department of Defense grant PR120935 (J.M. Maris), an Alex's Lemonade Stand Reach Award (J.M. Maris), and the Giulio D'Angio Endowed Chair (J.M. Maris). Resin and radiolabeling guidance was kindly provided by Progenics Pharmaceuticals, Inc., a Lantheus company.

The costs of publication of this article were defrayed in part by the payment of page charges. This article must therefore be hereby marked *advertisement* in accordance with 18 U.S.C. Section 1734 solely to indicate this fact.

### Note

Supplementary data for this article are available at Clinical Cancer Research Online (http://clincancerres.aacrjournals.org/).

Received March 9, 2022; revised June 9, 2022; accepted July 19, 2022; published first July 21, 2022.

## References


1. Maris JM. Recent advances in neuroblastoma. N Engl J Med 2010;362:2202–11.
2. Matthay KK, Maris JM, Schleiermacher G, Nakagawara A, Mackall CL, Diller L, et al. Neuroblastoma. Nat Rev Dis Primers 2016;2:16078.
3. Dubois SG, Geier E, Batra V, Yee SW, Neuhaus J, Segal M, et al. Evaluation of norepinephrine transporter expression and metaiodobenzylguanidine avidity in neuroblastoma: a report from the Children's Oncology Group. Int J Mol Imaging 2012;2012:250834.
4. Streby KA, Shah N, Ranalli MA, Kunkler A, Cripe TP. Nothing but NET: a review of norepinephrine transporter expression and efficacy of 131I-mIBG therapy. Pediatr Blood Cancer 2015;62:5–11.
5. DuBois SG, Matthay KK. Radiolabeled metaiodobenzylguanidine for the treatment of neuroblastoma. Nucl Med Biol 2008;35:S35–48.
6. Rutgers M, Buitenhuis CK, Hoefnagel CA, Voute PA, Smets LA. Targeting of meta-iodobenzylguanidine to SK-N-SH human neuroblastoma xenografts: tissue distribution, metabolism and therapeutic efficacy. Int J Cancer 2000;87:412–22.
7. Matthay KK, Tan JC, Villablanca JG, Yanik GA, Veatch J, Franc B, et al. Phase I dose escalation of iodine-131-metaiodobenzylguanidine with myeloablative chemotherapy and autologous stem-cell transplantation in refractory neuroblastoma: a new approaches to Neuroblastoma Therapy Consortium Study. J Clin Oncol 2006;24:500–6.
8. Matthay KK, Yanik G, Messina J, Quach A, Huberty J, Cheng SC, et al. Phase II study on the effect of disease sites, age, and prior therapy on response to iodine-131-metaiodobenzylguanidine therapy in refractory neuroblastoma. J Clin Oncol 2007;25:1054–60.
9. Yanik GA, Villablanca JG, Maris JM, Weiss B, Groshen S, Marachelian A, et al. 131I-metaiodobenzylguanidine with intensive chemotherapy and autologous stem cell transplantation for high-risk neuroblastoma. A new approaches to neuroblastoma therapy (NANT) phase II study. Biol Blood Marrow Transplant 2015;21:673–81.
10. Fishel Ben Kenan R, Polishchuk AL, Hawkins RA, Braunstein SE, Matthay KK, DuBois SG, et al. Anatomic patterns of relapse and progression following treatment with (131) I-MIBG in relapsed or refractory neuroblastoma. Pediatr Blood Cancer 2022;69:e29396.
11. Sgouros G, Roeske JC, McDevitt MR, Palm S, Allen BJ, Fisher DR, et al. MIRD Pamphlet No. 22 (abridged): radiobiology and dosimetry of alpha-particle emitters for targeted radionuclide therapy. J Nucl Med 2010;51:311–28.
12. Humm JL. Dosimetric aspects of radiolabeled antibodies for tumor therapy. J Nucl Med 1986;27:1490–7.
13. Vaidyanathan G, Zalutsky MR. Astatine radiopharmaceuticals: prospects and problems. Curr. Radiopharm 2008;1:177.
14. Tafreshi NK, Doligalski ML, Tichacek CJ, Pandya DN, Budzevich MM, El-Haddad G, et al. Development of targeted alpha particle therapy for solid tumors. Molecules 2019;24:4314.
15. Sgouros G, Bodei L, McDevitt MR, Nedrow JR. Radiopharmaceutical therapy in cancer: clinical advances and challenges. Nat Rev Drug Discov 2020;19:589–608.
16. Pouget JP, Constanzo J. Revisiting the radiobiology of targeted alpha therapy. Front Med 2021;8:692436.
17. Cunningham SH, Mairs RJ, Wheldon TE, Welsh PC, Vaidyanathan G, Zalutsky MR. Toxicity to neuroblastoma cells and spheroids of benzylguanidine conjugated to radionuclides with short-range emissions. Br J Cancer 1998;77:2061–8.
18. Strickland DK, Vaidyanathan G, Zalutsky MR. Cytotoxicity of alpha-particle-emitting m-[211At]astatobenzylguanidine on human neuroblastoma cells. Cancer Res 1994;54:5414–9.
19. Pozzi OR, Zalutsky MR. Radiopharmaceutical chemistry of targeted radiotherapeutics, part 4: strategies for 211At labeling at high activities and radiation doses of 211At alpha-particles. Nucl Med Biol 2017;46:43–9.
20. Vaidyanathan G, Affleck DJ, Alston KL, Zhao XG, Hens M, Hunter DH, et al. A kit method for the high level synthesis of [211At]MABG. Bioorg Med Chem 2007;15:3430–6.
21. Ohshima Y, Sudo H, Watanabe S, Nagatsu K, Tsuji AB, Sakashita T, et al. Antitumor effects of radionuclide treatment using alpha-emitting meta-(211)At-astato-benzylguanidine in a PC12 pheochromocytoma model. Eur J Nucl Med Mol Imaging 2018;45:999–1010.
22. Mairs RJ, Boyd M. Preclinical assessment of strategies for enhancement of metaiodobenzylguanidine therapy of neuroendocrine tumors. Semin Nucl Med 2011;41:334–44.
23. Ohshima Y, Kono N, Yokota Y, Watanabe S, Sasaki I, Ishioka NS, et al. Anti-tumor effects and potential therapeutic response biomarkers in alpha-emitting meta-(211)At-astato-benzylguanidine therapy for malignant pheochromocytoma explored by RNA-sequencing. Theranostics 2019;9:1538–49.
24. Vaidyanathan G, Friedman HS, Keir ST, Zalutsky MR. Evaluation of meta-[211At]astatobenzylguanidine in an athymic mouse human neuroblastoma xenograft model. Nucl Med Biol 1996;23:851–6.
25. Zalutsky MR, Reardon DA, Akabani G, Coleman RE, Friedman AH, Friedman HS, et al. Clinical experience with alpha-particle emitting 211At: treatment of recurrent brain tumor patients with 211At-labeled chimeric antitenascin monoclonal antibody 81C6. J Nucl Med 2008;49:30–8.
26. Andersson H, Cederkrantz E, Back T, Divgi C, Elgqvist J, Himmelman J, et al. Intraperitoneal alpha-particle radioimmunotherapy of ovarian cancer patients: pharmacokinetics and dosimetry of (211)At-MX35 F(ab')2–a phase I study. J Nucl Med 2009;50:1153–60.
27. Seo Y, Gustafson WC, Dannoon SF, Nekritz EA, Lee CL, Murphy ST, et al. Tumor dosimetry using [124I]m-iodobenzylguanidine microPET/CT for [131I]m-iodobenzylguanidine treatment of neuroblastoma in a murine xenograft model. Mol Imaging Biol 2012;14:735–42.
28. Dickson PV, Hamner B, Ng CY, Hall MM, Zhou J, Hargrove PW, et al. *In vivo* bioluminescence imaging for early detection and monitoring of disease progression in a murine model of neuroblastoma. J Pediatr Surg 2007;42:1172–9.
29. Rader J, Russell MR, Hart LS, Nakazawa MS, Belcastro LT, Martinez D, et al. Dual CDK4/CDK6 inhibition induces cell-cycle arrest and senescence in neuroblastoma. Clin Cancer Res 2013;19:6173–82.
30. Bankhead P, Loughrey MB, Fernandez JA, Dombrowski Y, McArt DG, Dunne PD, et al. QuPath: open source software for digital pathology image analysis. Sci Rep 2017;7:16878.
31. Progenics Pharmaceuticals, Inc. AZEDRA (iobenguane I 131) [package insert]. U.S. Food and Drug Administration website. Available from: https://www.accessdata.fda.gov/drugsatfda_docs/label/2018/209607s000lbl.pdf.
32. Batra V, Makvandi M, Zuppa AF, Patel N, Elias J, Pryma DA, et al. Dexmedetomidine does not interfere with meta-iodobenzylguanidine (MIBG) uptake at clinically relevant concentrations. Pediatr Blood Cancer 2017;64.
33. Makvandi M, Xu K, Lieberman BP, Anderson RC, Effron SS, Winters HD, et al. A radiotracer strategy to quantify PARP-1 expression *in vivo* provides a biomarker that can enable patient selection for PARP inhibitor therapy. Cancer Res 2016;76:4516–24.
34. Stabin MG, Sparks RB, Crowe E. OLINDA/EXM: the second-generation personal computer software for internal dose assessment in nuclear medicine. J Nucl Med 2005;46:1023–7.
35. McLendon RE, Archer GE, Garg PK, Bigner DD, Zalutsky MR. Radiotoxicity of systematically administered [211At]astatide in B6C3F1 and BALB/c (nu/nu) mice: a long-term survival study with histologic analysis. Int J Radiat Oncol Biol Phys 1996;35:69–80.
36. Kinuya S, Li XF, Yokoyama K, Mori H, Shiba K, Watanabe N, et al. Local delivery of (131)I-MIBG to treat peritoneal neuroblastoma. Eur J Nucl Med Mol Imaging 2003;30:1246–50.
37. Houghton PJ, Morton CL, Tucker C, Payne D, Favours E, Cole C, et al. The pediatric preclinical testing program: description of models and early testing results. Pediatr Blood Cancer 2007;49:928–40.
38. Rokita JL, Rathi KS, Cardenas MF, Upton KA, Jayaseelan J, Cross KL, et al. Genomic profiling of childhood tumor patient-derived xenograft models to enable rational clinical trial design. Cell Rep 2019;29:1675–89.
39. Batra V, Maris JM, Kang MH, Reynolds CP, Houghton PJ, Alexander D, et al. Initial testing (stage 1) of SGI-1776, a PIM1 kinase inhibitor, by the pediatric preclinical testing program. Pediatr Blood Cancer 2012;59:749–52.
40. Johnson K, McGlynn B, Saggio J, Baniewicz D, Zhuang H, Maris JM, et al. Safety and efficacy of tandem 131I-metaiodobenzylguanidine infusions in relapsed/refractory neuroblastoma. Pediatr Blood Cancer 2011;57:1124–9.
41. Kang TI, Brophy P, Hickeson M, Heyman S, Evans AE, Charron M, et al. Targeted radiotherapy with submyeloablative doses of 131I-MIBG is effective for disease palliation in highly refractory neuroblastoma. J Pediatr Hematol Oncol 2003;25:769–73.
42. Lumbroso J, Hartmann O, Schlumberger M. Therapeutic use of [131I]metaiodobenzylguanidine in neuroblastoma: a phase II study in 26 patients. "Societe Francaise d'Oncologie Pediatrique" and Nuclear Medicine Co-investigators. J Nucl Biol Med 1991;35:220–3.
43. Wilson JS, Gains JE, Moroz V, Wheatley K, Gaze MN. A systematic review of 131I-meta iodobenzylguanidine molecular radiotherapy for neuroblastoma. Eur J Cancer 2014;50:801–15.

44. Vaidyanathan G, Zalutsky MR. 1-(m-[211At]astatobenzyl)guanidine: synthesis via astato demetalation and preliminary *in vitro* and *in vivo* evaluation. Bioconjug Chem 1992;3:499–503.
45. Lindegren S, Albertsson P, Back T, Jensen H, Palm S, Aneheim E. Realizing clinical trials with astatine-211: the chemistry infrastructure. Cancer Biother Radiopharm 2020;35:425–36.
46. Ukon N, Zhao S, Washiyama K, Oriuchi N, Tan C, Shimoyama S, et al. Human dosimetry of free (211)At and meta-[(211)At]astatobenzylguanidine ((211)At-MABG) estimated using preclinical biodistribution from normal mice. EJNMMI Phys 2020;7:58.
47. Hallqvist A, Bergmark K, Back T, Andersson H, Dahm-Kahler P, Johansson M, et al. Intraperitoneal alpha-emitting radioimmunotherapy with (211)at in relapsed ovarian cancer: long-term follow-up with individual absorbed dose estimations. J Nucl Med 2019;60:1073–9.
48. Kunos CA, Mankoff DA, Schultz MK, Graves SA, Pryma DA. Radiopharmaceutical chemistry and drug development-what's changed? Semin Radiat Oncol 2021;31:3–11.
49. Makvandi M, Dupis E, Engle JW, Nortier FM, Fassbender ME, Simon S, et al. Alpha-emitters and targeted alpha therapy in oncology: from basic science to clinical investigations. Target Oncol 2018;13:189–203.
50. Eychenne R, Cherel M, Haddad F, Guerard F, Gestin JF. Overview of the most promising radionuclides for targeted alpha therapy: the "Hopeful Eight. Pharmaceutics 2021;13:906.